Desalination and Water Treatment
www.deswater.com

doi: 10.5004/dwt.2021.27404

229 (2021) 441–451
July

Efficient removal of carmoisine dye from aqueous solution using Fe_3O_4 magnetic nanoparticles modified with asparagine

Seyedeh Zahra Mostashari[a], Abdollah Fallah Shojaei[b,*], Khalil Tabatabaeian[b], Hassan Kefayati[c], Shahab Shariati[c]

[a]*Department of Chemistry, University Campus 2, University of Guilan, Rasht, Iran, email: szmostashari@gmail.com*
[b]*Department of Chemistry, Faculty of Sciences, University of Guilan, Rasht, Iran, Tel. +989112372711/+981333362207/ +981333402715; emails: a.f.shojaie@guilan.ac.ir (A.F. Shojaei), taba@guilan.ac.ir (K. Tabatabaeian)*
[c]*Department of Chemistry, Rasht Branch, Islamic Azad University, Rasht, Iran, emails: kefayati@iaurasht.ac.ir (H. Kefayati), shariaty@iaurasht.ac.ir (S. Shariati)*

Received 16 September 2020; Accepted 3 May 2021

ABSTRACT

In the present study, Fe_3O_4@SiO_2-NH_2-Asn magnetic nanoparticles (MNPs) were prepared and used for the first time as an efficient adsorbent for the removal of Carmoisine dye from aqueous solutions. Characterization of the synthesized adsorbent was performed by transmission electron microscopy, field emission scanning electron microscopy, Fourier transform infrared spectroscopy, X-ray diffraction, and vibrating sample magnetometer instruments. Taguchi experimental design method (OA_{16}) was utilized to evaluate the effect of adsorption parameters on the dye removal efficiency from aqueous solutions. Experimental results showed 96.6% removal efficiency of Carmoisine dye from aqueous solutions at pH = 3, adsorbent weight = 0.08 g, ionic strength = 0.05 mol L^{-1}, and contact time = 20 min. The adsorption isotherm studies with Freundlich, Langmuir, and Temkin isotherm models revealed that the adsorption data were best fitted to the Freundlich model (R^2 = 0.9989, n = 0.19), which showing multilayer adsorption of the dye on the adsorbent surface. The kinetic data were investigated by pseudo-first-order, pseudo-second-order, intra-particle diffusion, and Elovich kinetic models. According to obtained data, the pseudo-second-order kinetic model was the best model for describing the adsorption kinetic (R^2 = 0.9999). In addition, the Fe_3O_4@SiO_2-NH_2-Asn MNPs could be easily recovered by an external magnet and it displayed reusability for the subsequent seven runs. The results of Carmoisine removal from real samples showed that the Fe_3O_4@SiO_2-NH_2-Asn MNPs are appropriate adsorbents for the elimination of this pollutant from aqueous media.

Keywords: Asparagine; Carmoisine; Dye; Fe_3O_4@SiO_2-NH_2-Asn; Magnetite; Removal

1. Introduction

In the last years, protection of water has been a deepening worldwide challenge on account of growing water contamination and water reduction discharged (disposed) of the chemical industry with the process of urbanization and industrialization [1–3]. Different pollutants such as antibiotics, organic dyes, benzene, and its derivatives, and heavy metals, etc. would result in unavoidable influences on human health and even induce various crucial illnesses like cerebrovascular diseases, leukemia, cancer, etc. due to their toxicity of cumulation, mutagenicity, and even carcinogenicity [4–8]. Moreover, organic dyes could hardly be degraded with the conventional purification technique because of their low biodegradability and high dissolubility [9]. Carmoisine

* Corresponding author.

($C_{20}H_{12}N_2Na_2O_7S_2$) is a water-soluble, sulfonated, anionic, mono-azo dye that is utilized in producing sausages and confectionery products, marzipan, candies, jams, soups, sauces, sweets, preserves, beverages, and a variety of other foodstuffs. On account of the different utilizes of carmoisine in food processing, carmoisine is usually found in the food processing factories effluent [10]. Thus, researching and developing effective and economic decontamination technology to resolve the aforementioned pollutions from wastewater remains a great challenge in water treatment.

Traditional techniques like chemical oxidation, coagulation, photocatalysis, adsorption, and ion exchange have been utilized for eliminating organic dyes from polluted waters [11–16]. These techniques are restricted to several factors like the utilization of special equipment, high cost, dye incomplete elimination, and production of poisonous residues causing secondary pollution.

More consideration has lately been paid to the adsorption process because of its effectiveness, low cost, simplicity of design, and ease of operation [17–20]. This method can be employed for large-scale contaminated water repeatedly as it can handle fairly large flow rates, generating a high quality of water with no generating notorious sludge and residual contaminant. The development of dependable and cost-effective dye adsorbents has hence been a crucial issue to address.

The magnetic separation technique is affordable; it functions mainly in the swift adsorption of dyes [21,22]. Following the adsorption is completed using an external magnetic field, the adsorbents can be separated from the water system to avoid secondary pollution. The organic modified Fe_3O_4 nanocomposites are one of the most generally utilized magnetic materials, have been extensively utilized in lots of fields like magnetic resonance imaging, drug delivery, catalysis, and biotechnology [23–26]. Apart from this, organic modification Fe_3O_4 nano-composites had been broadly utilized in wastewater treatment because of their regeneration, easy separation, non-toxicity, and regeneration [26]. For instance, Toutounchi et al. [27] reported that magnetic ordered mesoporous carbon nanocomposite for the elimination of Ponceau 4R from the surface waters and dye industry. Cui et al. [28] reported urchin-like Fe_3O_4@PDA-Ag hollow microspheres could boost the efficiency of removal of rhodamine B and methylene blue from wastewater.

In this research, we have successfully fabricated Fe_3O_4@SiO_2-NH_2-Asn MNPs with a simple route and investigated MNPs performance for removal of Carmoisine dye from aqueous solutions. The effect of parameters affecting the adsorption of Carmoisine onto Fe_3O_4@SiO_2-NH_2-Asn, including the initial solution pH, ionic strength, adsorbent amount, and contact time, were systematically examined by batch adsorption experiments. The characteristic reflects that the Fe_3O_4@SiO_2-NH_2-Asn could be a high-efficiency adsorbent for the removal of Carmoisine from an aqueous solution.

2. Experimental

2.1. Chemicals and reagents

Ferrous chloride tetrahydrate ($FeCl_2{\cdot}4H_2O$) (≥98.0%), ferric chloride hexahydrate ($FeCl_3{\cdot}6H_2O$), hydrochloric acid (HCl) (37%, w/w), ammonia solution (25%, w/w), ethanol, toluene, sodium chloride (NaCl), and Carmoisine were purchased from Merck Company (Darmstadt, Germany). Tetraethyl orthosilicate (TEOS) (98%), (3-aminopropyl) triethoxysilane (APTES) (99%), and L-Asparagine (≥98% (HPLC)) were bought from Sigma Company (Milwaukee, WI, USA). All chemical materials and solvents were used without further purification.

2.2. Instruments and apparatus

Fourier transform infrared (FT-IR) spectra were acquired in the range of 400–4,000 cm^{-1}, with a Shimadzu FT-IR 8600 spectrophotometer (Japan). The crystal phases of the prepared MNPs were evaluated at a scanning speed of 2°min^{-1} from 10° to 80° (2θ), utilizing Philips Xpert X-ray powder diffraction (XRD) diffractometer (Cu K_α radiation, λ = 0.154056 nm, Netherlands). The size and morphology of the synthesized MNPs were studied utilizing the field-emission scanning electron microscopy (FESEM, Sigma-VP, Zeiss Company, Germany). The structural characteristics of the adsorbent were investigated utilizing transmission electron microscopy (TEM) with the Zeiss-EM10C device. A vibrating sample magnetometer (VSM, LDJ9600) was utilized for investigating the magnetic properties of fabricated MNPs. UV-vis spectra were recorded using Cary 60 UV-vis Spectrophotometer from Agilent Technologies (USA) equipped with a quartz cell. The pH of solutions was measured utilizing Bante 901 digital pH meter (China). For magnetic separation, a super-strong magnet (1 cm × 3 cm × 5 cm) with a 1.4 T magnetic field was employed. To investigate the surface charges of synthesized adsorbent, Zeta potential analyzer (Malvern Instruments Ltd., Malvern, United Kingdom) was used.

2.3. Preparation of Fe_3O_4@SiO_2-NH_2-Asn MNPs

2.3.1. Synthesis of Fe_3O_4

Fe_3O_4 MNPs were prepared via the co-precipitation method described in the literature. Briefly, $FeCl_2{\cdot}4H_2O$ (6.0 g), $FeCl_3{\cdot}6H_2O$ (9.3 g), and HCl 37% (4.5 mL) were dissolved in distilled water and the solution was adjusted to the mark of a 50 mL volumetric flask. Then, the solution was degassed for 20 min utilizing N_2 gas. In the next step, 250 mL of ammonia solution (1.5 mol L^{-1}) was added into a three-necked flask containing a magnet and was heated to 80°C in the oil bath. The solution of iron chlorides was added drop by drop to the solution of ammonia in a degassed environment for 60 min. After completion of the reaction, the MNPs were rinsed with double distilled water several times and were separated from the reaction environment with a super-strong magnet (1.4 T). The fabricated MNPs were kept in NaOH (0.1 mol L^{-1}) solution (24 h) to avoid the accumulation of MNPs. Finally, MNPs were rinsed with distilled water and were dried at 120°C in the oven for 120 min [29,30].

2.3.2. Aminopropyl surface modification of the Fe_3O_4 to form Fe_3O_4@SiO_2-NH_2

For silica coating, first, 0.7 g Fe_3O_4 was added in a solution containing ethanol (40 mL), 10 mL distilled water, and 0.6 mL ammonia solution, and then the solution was sonicated for 30 min at 80°C. Afterward, 0.5 mL TEOS was added to the suspension and the mixture was strongly stirred at room temperature (r.t, 24 h). The mixture was separated by a magnet and rinsed three times with a 1:1 mixture of distilled water/ethanol, and finally dried at 70°C for 5 h. In the next step, for the synthesis of Fe_3O_4@SiO_2-NH_2, a suspension including 1.0 g of Fe_3O_4@SiO_2 in 100 mL toluene was sonicated (30 min). Next, 1 mL of APTES was added to the suspension, and the mixture was stirred for 24 h at r.t. The mixture was separated by a magnet and rinsed three times with toluene/ethanol (1:1), and finally dried at 70°C for 8 h.

2.3.3. Synthesis of Fe_3O_4@SiO_2-NH_2-Asn

The synthesized Fe_3O_4@SiO_2-NH_2 MNPs were functionalized with Asparagine. First, a suspension of 0.8 g Fe_3O_4@SiO_2-NH_2 and 3.3 g Asparagine in 40 mL ethanol was sonicated for 10 min. Then, the mixture was refluxed for 8 h (80°C). Finally, the nanoparticles were washed with ethanol and dried in an oven (Fig. 1).

3. Results and discussion

3.1. Characterization of Fe_3O_4@SiO_2-NH_2-Asn

Characterization of the fabricated Fe_3O_4@SiO_2-NH_2-Asn was performed by several physicochemical methods such as FESEM, TEM, FT-IR, XRD, and VSM.

FESEM image of the prepared Fe_3O_4@SiO_2-NH_2-Asn MNPs is demonstrated in Fig. 2. As can be seen from Fig. 2, the synthesized MNPs have good morphology with dimensions between 21 and 66 nm.

The size and shape of the resulting adsorbent were further studied by TEM (Fig. 3). As can be observed, the synthesized MNPs have good core-shell structures and were composed of aggregated spherical particles with sizes below 30 nm. Furthermore, numerous nanoparticles are encapsulated in the SiO_2.

The FT-IR spectra of the Fe_3O_4, Fe_3O_4@SiO_2, Fe_3O_4@SiO_2-NH_2, asparagine, and Fe_3O_4@SiO_2-NH_2-Asn are displayed in Fig. 4. The band at 554 cm^{-1} corresponds to the stretching vibration of the Fe–O bond of Fe_3O_4. In addition, the peaks at 1,631 and 3,354 cm^{-1} are attributed to the stretching vibration of the hydroxyl (–OH) groups on the surface of the Fe_3O_4 nanoparticles (Fig. 4a). Furthermore, Fig. 4b attributed to Fe_3O_4@SiO_2, the band that appeared at 1,070 cm^{-1} is corresponding to Fe–O–Si. Fig. 4c shows characteristic bands of both Fe_3O_4 and amino groups in Fe_3O_4@SiO_2-NH_2. The bands at 2,804 and 1,582 cm^{-1} can be ascribed to the NH bending. In the spectrum of Asparagine

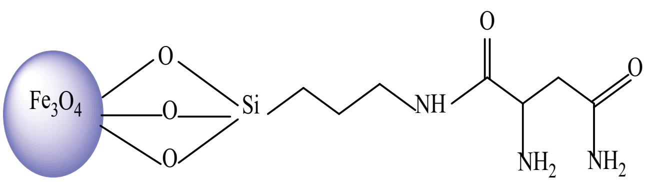

Fig. 1. Schematical structure of Fe_3O_4@SiO_2-NH_2-Asn MNPs.

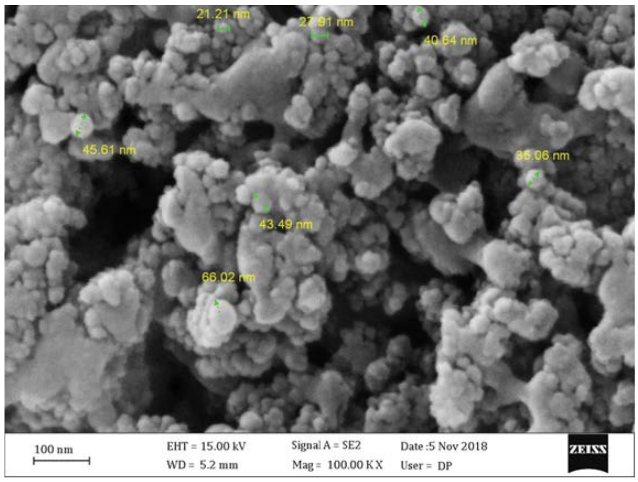

Fig. 2. FESEM image of synthesized Fe_3O_4@SiO_2-NH_2-Asn MNPs.

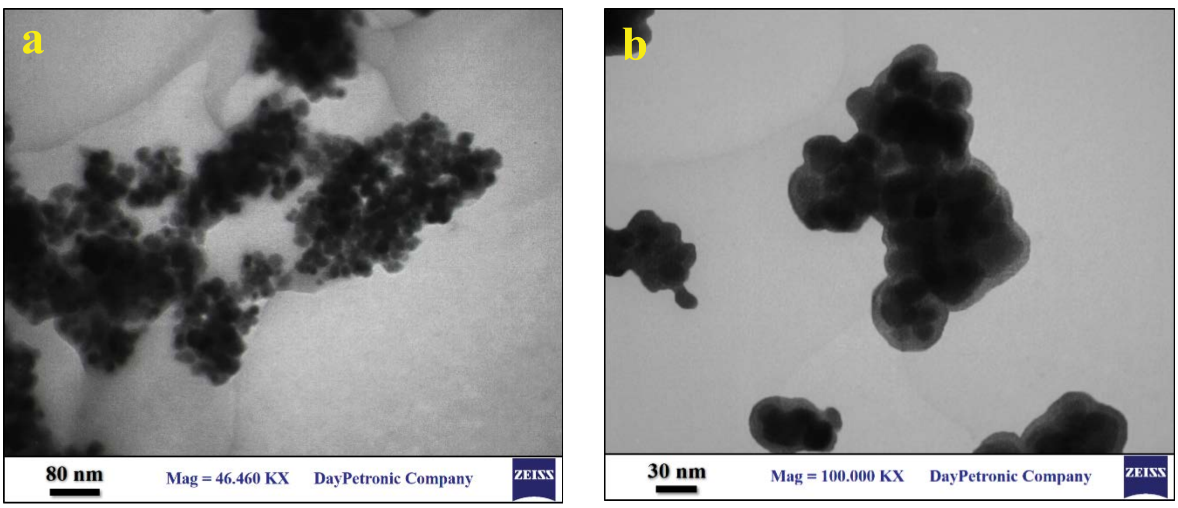

Fig. 3. TEM micrograph of Fe_3O_4@SiO_2-NH_2-Asn at different magnifications (a and b).

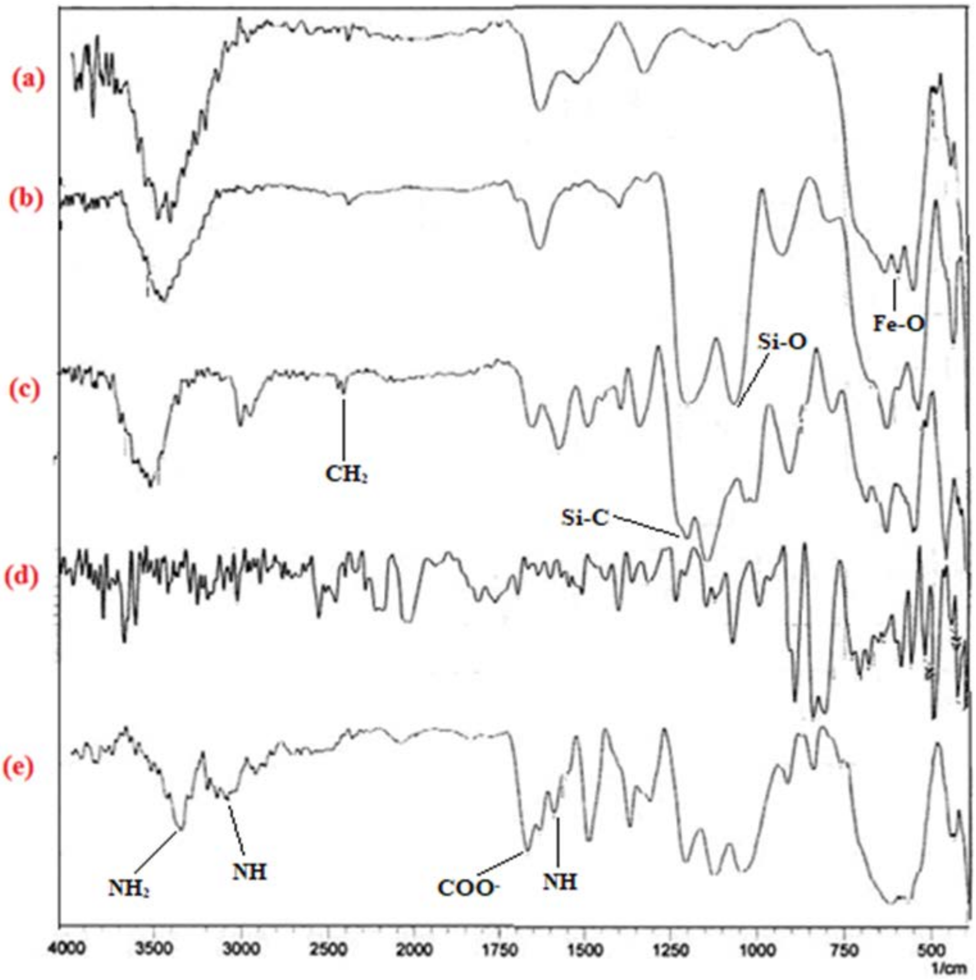

Fig. 4. FT-IR spectra of (a) Fe_3O_4, (b) Fe_3O_4@SiO_2, (c) Fe_3O_4@SiO_2-NH_2, (d) Asparagine, and (e) Fe_3O_4@SiO_2-NH_2-Asn MNPs.

(Fig. 4d), the bands that emerged at 3,207 cm^{-1} are ascribed to the NH stretching vibration of the amino group. The bands at 1,751 and 1,502 cm^{-1} belong to the symmetric and asymmetric stretching vibrations of COO^-. The strong absorption band at 580 cm^{-1} is corresponding to the Fe–O bond stretching vibration of Fe_3O_4, which confirms the existence of asparagine on the Fe_3O_4 surface.

X-ray diffraction (XRD) pattern of synthesized Fe_3O_4@SiO_2-NH_2-Asn MNPs is demonstrated in Fig. 5. As illustrated in Fig. 5, the six characteristic dominant XRD peaks are located at 2θ = 30.29°, 35.67°, 37.50°, 43.35°, 53.74°, 57.29°, 62.92°, and 74.63° which can be relevant to (220), (222), (300), (400), (422), (511), (440), and (622) planes of Fe_3O_4, respectively (JCPDS No. 19-692). These peaks are well-defined and confirm the well-crystallized structure of Fe_3O_4 with a typical cubic spinel phase. This result corroborated the existence of magnetite core in the structure of prepared MNPs.

The vibrating sample magnetometer (VSM) curve of the Fe_3O_4@SiO_2-NH_2-Asn MNPs is demonstrated in Fig. 6. VSM measurement was carried out by taking the solid sample on the tips of the vibrating rod and analyzing it at r.t in an applied magnetic field sweeping from −20 to 20 kOe. The saturated magnetization value of

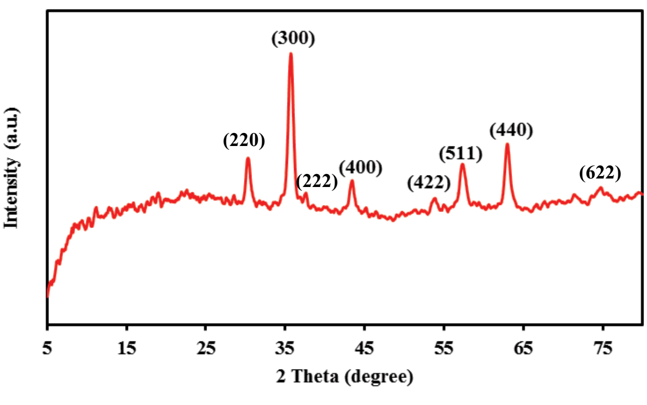

Fig. 5. XRD diffraction pattern of synthesized Fe_3O_4@SiO_2-NH_2-Asn MNPs.

Fe_3O_4@SiO_2-NH_2-Asn MNPs was 47.1 emu g^{-1} which indicates the synthesized Fe_3O_4@SiO_2-NH_2-Asn MNPs have a proper magnetic response to the magnetic fields.

To study the surface charge of synthesized MNPs which can affect their physical stability in solution, zeta-potential as an indirect measuring the net charge on the surface of NPs was measured utilizing a particle

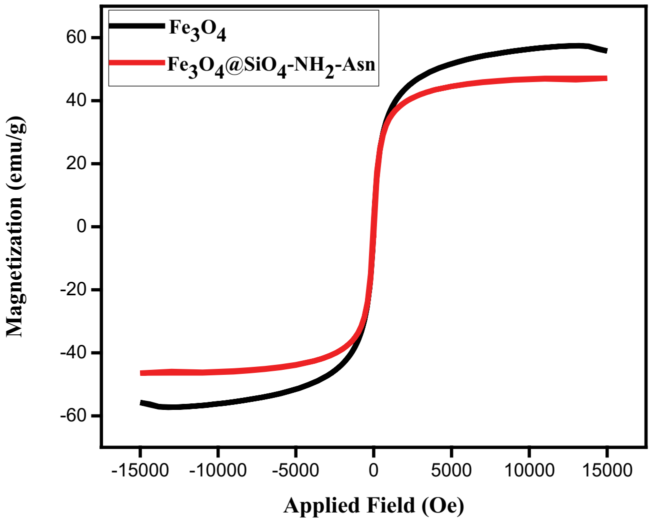

Fig. 6. VSM of pure Fe_3O_4 and Fe_3O_4@SiO_2-NH_2-Asn MNPs.

Charge Reader. Its value is utilized as a dispersion stability index and can be utilized to specify the particles' tendency to aggregate in the aqueous medium. In the present research, the zeta potential and mobility were measured as 31.1 mv and 2.44 μm cm Vs^{-1}, respectively at 298 K with a count rate of 172.4 kcps (Fig. 7). The large zeta potential obtained in this study predicts a more stable dispersion of synthesized MNPs and shows the positive charge of the surface of MNPs that makes it suitable for electrostatic interaction with anionic dye.

3.2. Carmoisine adsorption optimization

All the batch mode tests were performed by agitating a certain quantity of adsorbent in 50 mL of dye solution of favored concentration, contact time, pH, and ionic strength in a beaker. The pH effect on the adsorption of Carmoisine dye was assessed on the pH range of 1–6. The pH was adjusted utilizing 0.1 mol L^{-1} HCl or NaOH solutions. The effect of adsorbent mass on the elimination of Carmoisine was analyzed in the range of 0.02–0.11 g per 50 mL dye (40 mg L^{-1}) at pH 7 for 50 min. Batch equilibrium adsorption experiments were conducted by contacting 50 mL of 40 mg L^{-1} Carmoisine solution with 0.11 g of the adsorbent for 20 min at r.t and pH 6. The samples were agitated and withdrawn from the beaker at pre-determined time intervals. The adsorbent was separated from the solution of dye by a magnet. The concentration of the supernatant was measured utilizing a UV-vis spectrophotometer as given in section 2.3 (Preparation of Fe_3O_4@SiO_2-NH_2-Asn MNPs). According to obtained results, 513 nm was selected as the best wavelength for quantitative measurements (Fig. 8). The removal percentage of the Carmoisine in solution was calculated utilizing the following equation:

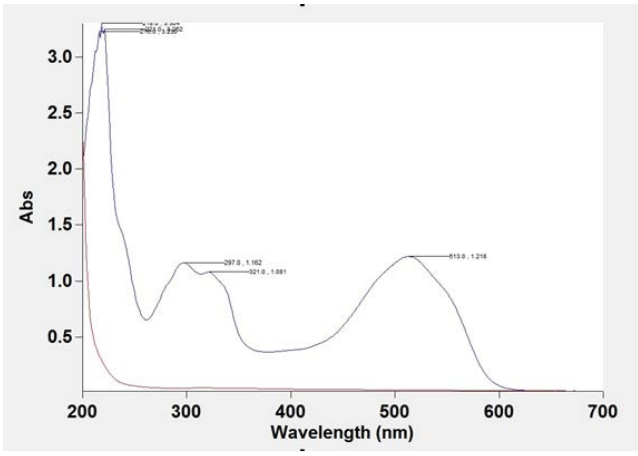

Fig. 8. UV-vis spectra of Carmoisine before and after removal by Fe_3O_4@SiO_2-NH_2-Asn MNPs.

$$\%\text{Removal efficiency} = \frac{C_0 - C_t}{C_0} \times 100 \tag{1}$$

where C_0 and C_t are initial and equilibrium concentrations of Carmoisine after treatment with adsorbent, respectively.

3.3. Taguchi method for Carmoisine adsorption optimization

To obtain better removal efficiency of Carmoisine from aqueous solutions, the experimental conditions were optimized using orthogonal Taguchi array design to achieve the optimum experimental parameters with a minimum number of experiments. For this purpose, different conditions affecting the adsorption process such as adsorbent weight (0.02, 0.05, 0.08, and 0.11 g), contact time (5, 10, 15, and 20 min), ionic strength (0, 0.01, 0.05, and 0.2 mol L^{-1})

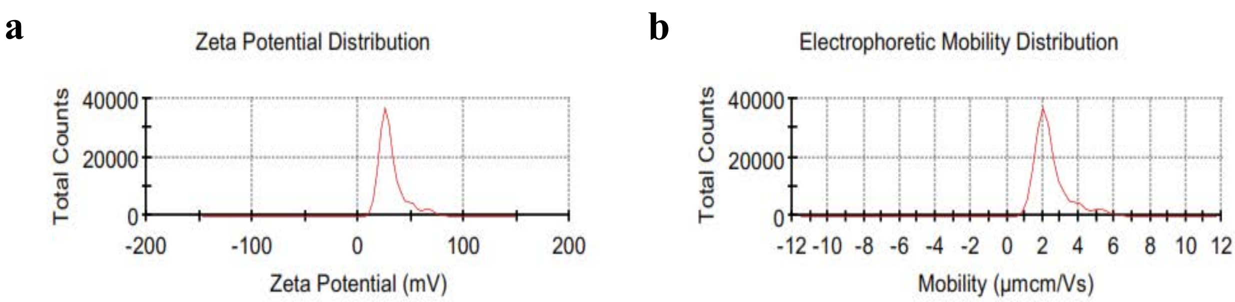

Fig. 7. Zeta potential distribution (a), and electrophoretic mobility distribution (b) of MNPs.

and solution pH (3, 4, 5, and 6) were investigated at four levels at constant volume of 50 mL and 40 mg L^{-1} Carmoisine concentration (Table 1).

One of the crucial parameters in the adsorption procedure is the primary pH value of the solution which needs to be optimized to achieve desirable adsorption efficiency. In the present research, the effect of pH on Carmoisine dye adsorption efficiencies was examined in the pH range of 1–6. Optimization experiments were performed in accordance with the following procedure. First, the pH of the Carmoisine dye solution (40 mg L^{-1}) was adjusted and the absorbance was recorded by spectrophotometer. Next, a certain amount of Fe_3O_4@SiO_2-NH_2-Asn adsorbent was added to the solution and stirred for a while on a magnetic stirrer. After that, the container containing the solution was placed on a super magnet to separate and remove the adsorbent from the solution. The separated solution was transferred to the quartz cell and its absorbance was recorded by a spectrophotometer at 513 nm (Fig. 8). In accordance with the results, the Carmoisine dye sorption by Fe_3O_4@SiO_2-NH_2-Asn was more effective at a pH range of 2–6. However, by enhancing the solution pH, the elimination efficiency was reduced. Greater Carmoisine removal under an acidic medium can be owing to the protonation of the surface of the adsorbent and electrostatic interactions between the anionic dye molecules and adsorbent that facilitates the diffusion process.

The adsorbent amount is one of the crucial factors in the adsorption process. To investigate this factor, the adsorbent amounts of 0.02 (0.4 g L^{-1}), 0.05 (1.0 g L^{-1}), 0.08 (1.6 g L^{-1}), and 0.11 g (2.2 g L^{-1}) were considered (Fig. 9). According to the results, the optimum adsorbent weight was obtained to be 0.08 g (1.6 g L^{-1}). Because there are more available active sites for Carmoisine adsorption, the removal efficiency increases by increasing in an adsorbent amount from 0.4 to 1.6 g L^{-1}. The dye removal efficiency was decreased in higher adsorbent amounts (2.2 g L^{-1}). This can be caused by the high adsorbent concentration for this purpose and excess particle interactions, like aggregation, that would result in a reduction in the total surface area of the adsorbent [31].

The influence of contact time of Fe_3O_4@SiO_2-NH_2-Asn MNPs on Carmoisine removal efficiency was examined in the range of 5, 10, 15, and 20 min (Fig. 9). It was seen that the removal efficiency of Carmoisine was enhanced at 20 min. In fact, with increasing contact time there are more opportunities for Carmoisine ions to contact with the adsorbent surface.

To investigate the ionic strength effect on the removal of Carmoisine using Fe_3O_4@SiO_2-NH_2-Asn MNPs, NaCl was

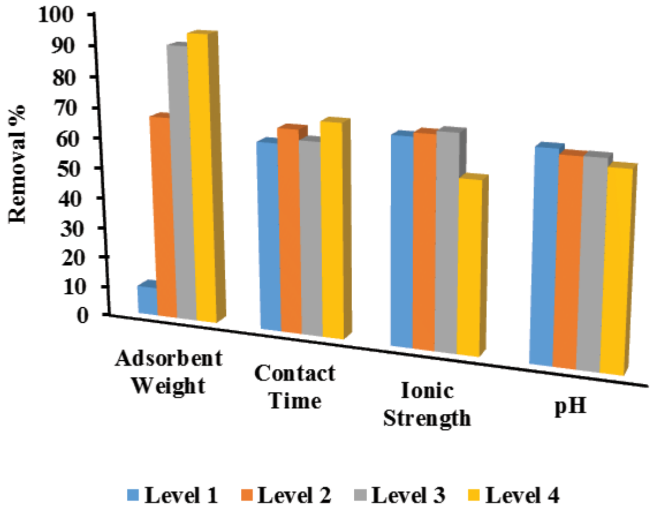

Fig. 9. Influence of adsorbent weight, contact time, ionic strength, and pH on Carmoisine removal percentage.

Table 1
Design of experiments by OA16 matrix for Carmoisine

Run	Adsorbent amount (g)	pH	Contact time (min)	Ionic strength (mol L^{-1})	Removal (%)
1	0.02	3	5	0	3.8
2	0.05	3	10	0.01	78.3
3	0.08	3	15	0.05	95.78
4	0.11	3	20	0.2	90.8
5	0.02	4	15	0.01	10.5
6	0.05	4	20	0	74.8
7	0.08	4	5	0.2	2.45
8	0.11	4	10	0.05	94.5
9	0.02	5	20	0.05	23.3
10	0.05	5	15	0.2	49.9
11	0.08	5	10	0	93.5
12	0.11	5	5	0.01	95.8
13	0.02	6	10	0.2	0
14	0.05	6	5	0.05	65
15	0.08	6	20	0.01	89.8
16	0.11	6	15	0	97

added to the solution at concentrations of 0, 0.01, 0.05, and 0.2 mol L^{-1}. As displayed in Fig. 9, the optimum amount of ionic strength was 0.05 mol L^{-1}. The results revealed that with the increase in ionic strength from 0 to 0.05 mol L^{-1}, the removal efficiency of adsorbent is increased which may be because of reduced solubility of the Carmoisine dye in water and improvement of the interaction between the dye and the Fe_3O_4@SiO_2-NH_2-Asn MNPs in the ionic medium [24]. In higher ionic strength (0.2 mol L^{-1}), salt addition had a negative effect on the removal efficiency. This corresponded to Carmoisine dye molecules and salt ions competition for the sorption on the surface of Fe_3O_4@SiO_2-NH_2-Asn.

Carmoisine has sulfonic acid functional groups. In solution, it produces protons and negative ions. Also at acidic pHs, NH_2 groups of Fe_3O_4@SiO_2-NH_2-Asn MNPs are protonated to form NH_3^+. In this study, acidic pHs of 3, 4, 5, and 6 were selected to optimize the effect of solution pH. As revealed in Fig. 9, the maximum adsorption capacity of Carmoisine is recorded at pH = 3. At this pH, the anionic Carmoisine is electrostatically adsorbed to the surface of Fe_3O_4@SiO_2-NH_2-Asn MNPs.

To explore the repeatability of the removal process under optimal conditions (pH = 3, adsorbent weight = 0.08 g, ionic strength = 0.05 mol L^{-1}, and contact time = 20 min), this pattern was repeated three times and the mean removal efficiency was acquired about 96.6% ± 0.08%.

3.4. Adsorption isotherms

Adsorption isotherms, which illustrate the correlation between the equilibrium concentration of the adsorbate in the solution and on the adsorbent surface at a constant temperature, are usually employed to describe the adsorption process.

Here, to determine the adsorption isotherms, Temkin, Langmuir, and Freundlich adsorption isotherm models, were investigated (Fig. 10). Optimum conditions were obtained at different Carmoisine concentrations of 1, 5, 10, 25, 40, 75, 100, and 250 mg L^{-1} at room temperature. Then, the absorbance of the residual solution was recorded at each concentration by UV-vis spectrophotometer.

Langmuir equations can be expressed as Eq. (2):

$$\frac{C_e}{q_e} = \frac{C_e}{q_{\max}} + \frac{1}{Kq_{\max}} \quad (2)$$

where q_e, and C_e, respectively, refer to the mass of Carmoisine adsorbed onto the adsorbent in mg g^{-1}, and the equilibrium concentration of Carmoisine in mg L^{-1}, K, and $q_{\max}$

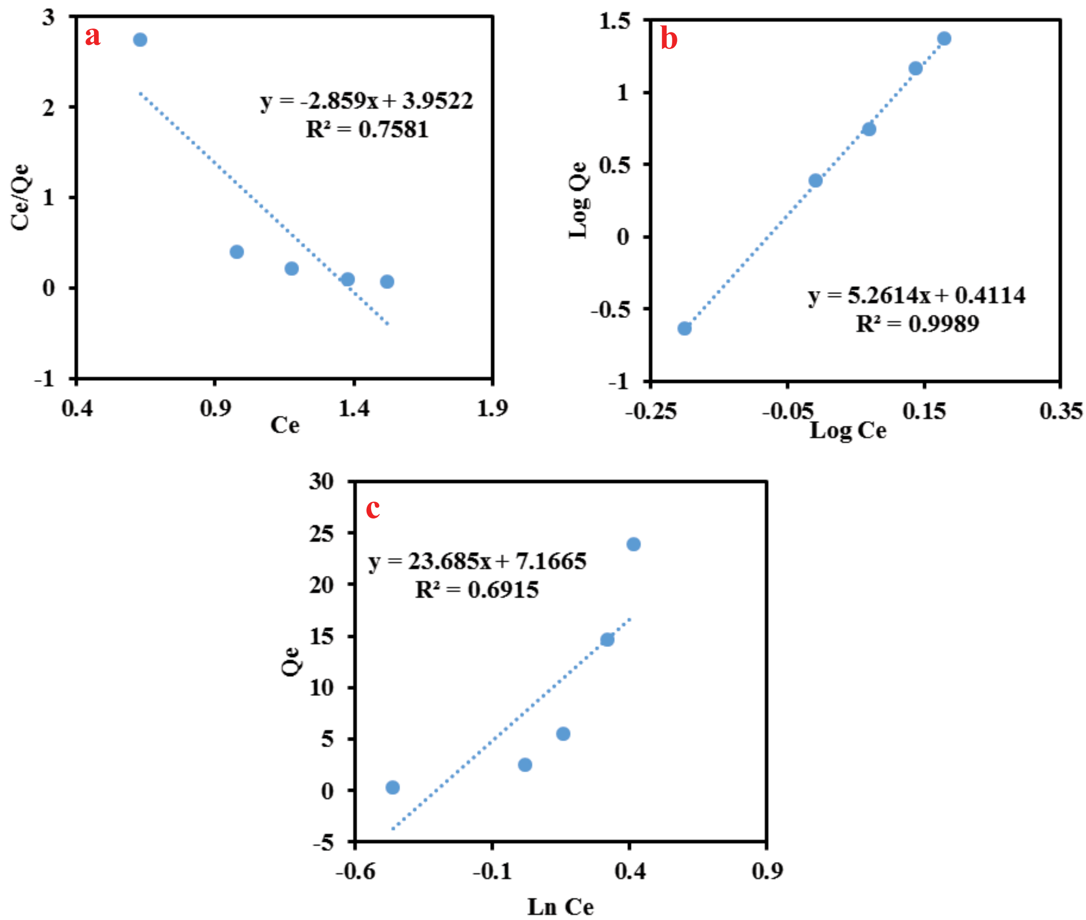

Fig. 10. (a) Langmuir, (b) Freundlich, and (c) Temkin adsorption isotherm plots for the removal of Carmoisine (pH = 3; adsorbent dose = 0.08 g; contact time = 20 min; ionic strength = 0.05 mol L^{-1}).

are, respectively, the adsorption equilibrium constant in terms of L mg^{-1}, and the maximum adsorption capacity in terms of mg g^{-1}.

As shown in Fig. 10a, adsorption data does not match with the Langmuir isotherm (R^2 = 0.7581).

Freundlich isotherm is commonly represented by Eq. (3):

$$\log q_e = \log K_F + \frac{1}{n_F} \log C_e \quad (3)$$

where q_e is the value of adsorbed Carmoisine at equilibrium (mg g^{-1}); K_F and n are, respectively, the Freundlich constants showing the adsorption capacity and the adsorption intensity, and also C_e is an aqueous concentration of adsorbate at equilibrium (mg L^{-1}).

Temkin isotherm [32] is described by the following equation:

$$q_e = K_1 \ln(K_2) + K_1 \ln(C_e) \quad (4)$$

where K_2 and K_1 are, respectively, the dimensionless Temkin isotherm constant, and related to the heat of adsorption (L g^{-1}) (Fig. 10c). Based on the correlation coefficient of this model (R^2 = 0.6915), the removal of Carmoisine ions was not matched by this model.

The investigation of the adsorption isotherms, Langmuir, Freundlich, and Temkin models was demonstrated in Fig. 10, and the determined values for the three model's parameters are presented in Table 2. The outcomes revealed that the experimental data for Carmoisine adsorption onto the Fe_3O_4@SiO_2-NH_2-Asn is fitted with the Freundlich isotherm model with R^2 values of 0.9989 which is better compared to the obtained values by the Langmuir and Temkin isotherm models. In the current research, the outcomes of fitting experimental data demonstrate which the adsorption of the Carmoisine is carried out by the sites of the adsorbent which are heterogeneous, signifying non-uniform, and multi-layer adsorption.

3.5. Kinetic study

To investigate the kinetics of Carmoisine dye removal by synthetic Fe_3O_4@SiO_2-NH_2-Asn MNPs, designed experiments were accomplished under optimum conditions at 40 mg L^{-1} of dye in 0–90 min (Fig. 11).

In this research, various models including Lagergren's pseudo-first-order, pseudo-second-order, intra-particle, and Elovich kinetic models were investigated (Figs. 12a–d). Kinetic studies were performed at optimal conditions and the solutions were stirred in time intervals ranged from 0 to 90 min. In different studied kinetic models, as shown in Fig. 12b, the best model was chosen based on the linear regression correlation coefficient (R^2 values). Regarding the high regression coefficient of the pseudo-second-order kinetic model (R^2 = 0.999), the kinetic of the Carmoisine adsorption process is best described by this model (Table 3). It demonstrates that chemisorption occurs during the adsorption of the Carmoisine on the surface of Fe_3O_4@SiO_2-NH_2-Asn MNPs.

In accordance with the calculated results, the maximum adsorption capacity of the Fe_3O_4@SiO_2-NH_2-Asn was estimated to be 24.1 mg g^{-1}.

3.6. Applicability of adsorbents for removal of Carmoisine from real samples

To explore the reliability and applicability of the synthesized Fe_3O_4@SiO_2-NH_2-Asn MNPs for dye removal in aqueous solutions, five aqueous samples with various matrixes including river water (Zarjoob River, Rasht, Iran), seawater (Caspian Sea, Ghazian, Iran), tap water (Rasht, Guilan, Iran), lagoon water (Anzali, Iran), and sand wastewater (Rasht, Iran) were collected from Guilan Province in Iran. To study the matrix impact of each sample on the removal efficiency of dye, the samples were spiked by Carmoisine individually, in such a way the final concentration of Carmoisine was fixed at 40 mg L^{-1}. The spiked samples were acted in the proposed removal process under optimized conditions (adsorbent weight = 0.08 g, pH = 3, ionic strength = 0.05 mol L^{-1}, and time = 20 min). Results showed good removal efficiency of Carmoisine in tap water (95%), seawater (74%), lagoon water (99%), Zarjoob river water (90%), and sand wastewater (74%) and confirming the potential of the synthesized MNPs for removal of Carmoisine dye from real water samples.

3.7. Reusability of Fe_3O_4@SiO_2-NH_2-Asn MNPs

To investigate the reusability ability of Fe_3O_4@SiO_2-NH_2-Asn MNPs, different repetitive Carmoisine adsorption tests

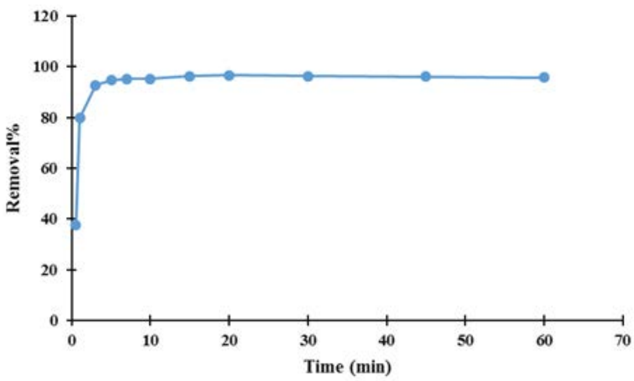

Fig. 11. Carmoisine removal percentage.

Table 2
Adsorption isotherms for adsorptive removal of Carmoisine

Temkin			Freundlich			Langmuir		
R^2	K_2	K_1	R^2	n	K_F	R^2	q_m	K
0.6915	1.34	23.68	0.9989	0.19	2.57	0.7581	–0.34	–0.72

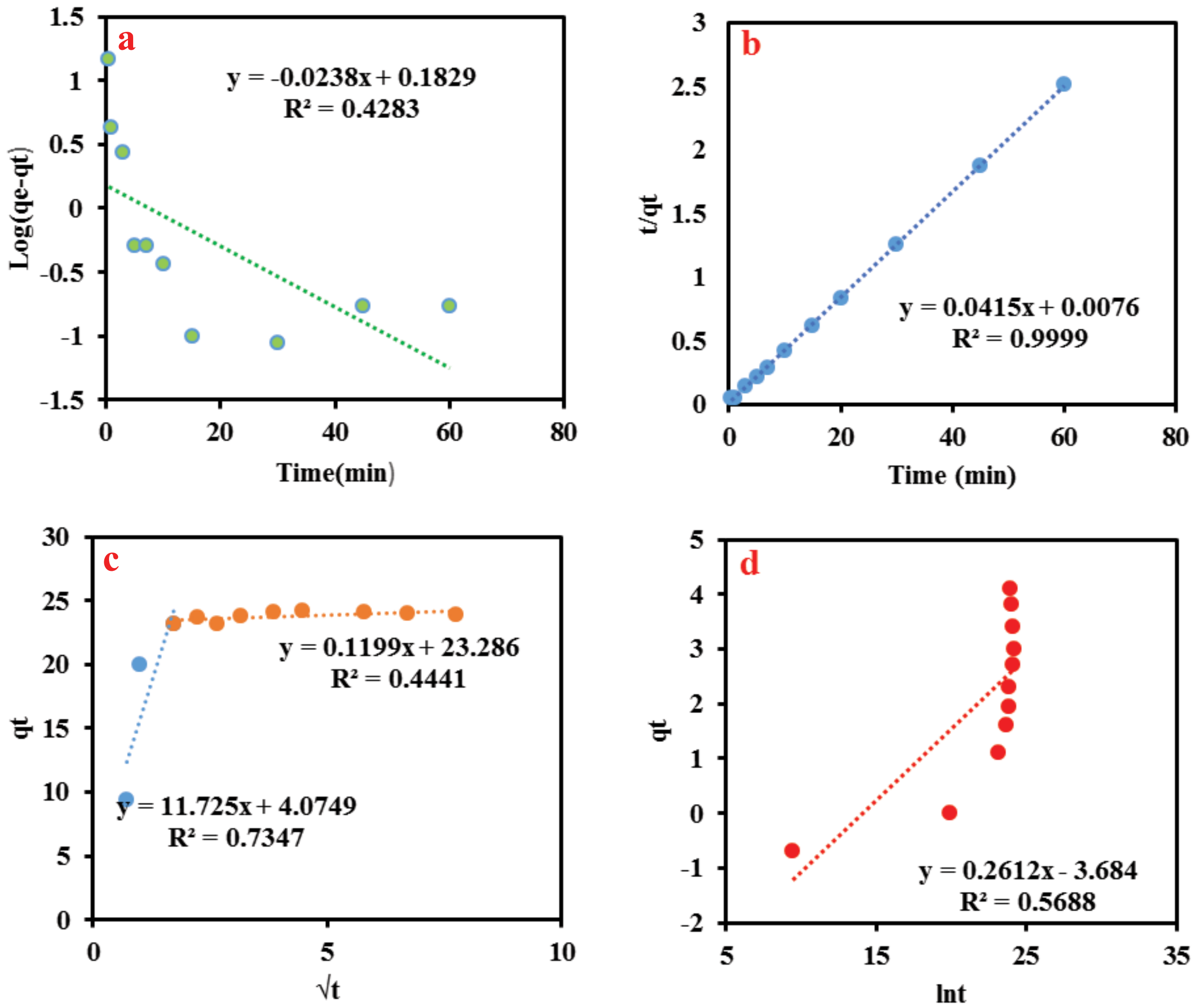

Fig. 12. (a) Pseudo-first-order, (b) pseudo-second-order, (c) intra particle, and (d) Elovich kinetic models.

Table 3
Kinetic study for adsorptive removal of Carmoisine

Elovich			Intra particle kinetic			Pseudo-second-order			Pseudo-first-order		
R^2	α	β	R^2	C	K_{ip}	R^2	q_e	K_2	R^2	q_e	K_1
0.5688	3×10^{-6}	3.8	0.4441 0.7347	23.286 4.079	0.1199 11.725	0.9999	24.1	0.22	0.4283	1.19	0.023

were performed at optimum conditions utilizing the same adsorbent. Dye desorption experiments were performed using NaOH (0.1 mol L^{-1}) for washing and removing the dye molecules from the adsorbent and finally drying the adsorbent to regenerate it at 100°C. After seven successive runs, the high magnetic sensitivity of recycled Fe_3O_4@SiO_2-NH_2-Asn MNPs still retained and the MNPs can be collected from the solution using a super magnet. As demonstrated in Fig. 13, after the seventh cycle, the adsorption efficiency for Carmoisine reduced from 96.6% to 79%. The results show an efficacious regeneration of the Fe_3O_4@SiO_2-NH_2-Asn by NaOH (0.1 mol L^{-1}) solution and reuse with an insignificant decrease in its adsorption efficiency that can corroborate the economical of the adsorption process.

3.8. Comparison with other adsorbents

Carmoisine removal efficiency by Fe_3O_4@SiO_2-NH_2-Asn was compared with previously reported adsorbents, and

Table 4
Comparison of maximum adsorption capacity of Carmoisine in various adsorbents

Adsorbents	Dye	Kinetic model	Isothermic model	q_{max} (mg g^{-1})	Ref.
Fe_3O_4@SiO_2-CMK-8 MNCs	Ponceau 4R	Pseudo-second order	Freundlich	78.74	[27]
Fe_3O_4@SiO_2@NH_2	Methyl red	Pseudo-second-order	Langmuir	125	[33]
Methyl propylaminopropanoate-coated Fe_3O_4@SiO_2 nanoparticles	Acid red 114	Pseudo-second-order	Langmuir	105	[34]
Fe_3O_4@SiO_2 nanospheres	Congo red	Pseudo-second-order	Langmuir	50	[35]
Fe_3O_4@SiO_2-NH_2-Asn	Carmoisine	Pseudo-second-order	Freundlich	24.1	Present work

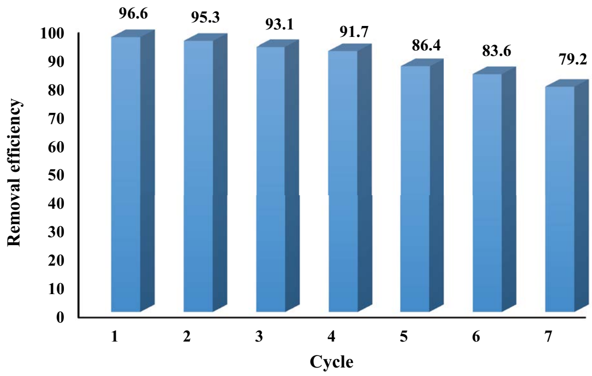

Fig. 13. Reusability of Fe_3O_4@SiO_2-NH_2-Asn for adsorption of the Carmoisine.

the results are demonstrated in Table 4. The results show that the Fe_3O_4@SiO_2-NH_2-Asn for Carmoisine removal was proper and exhibited satisfactory removal performance for Carmoisine.

4. Conclusions

This research revealed the application of Fe_3O_4@SiO_2-NH_2-Asn MNPs for the removal of the anionic Carmoisine dye from aqueous solutions. The highest removal efficiency for Carmoisine dye (~96.6%) was achieved at pH = 3, 0.08 g of Fe_3O_4@SiO_2-NH_2-Asn MNPs and 20 min. A study of kinetic models displayed that adsorption of Carmoisine is obeyed from pseudo-second-order kinetic model showing chemisorption. The Freundlich isotherm demonstrated the best interpretation of the results. Short adsorption time, separation with an external magnet, reusability, and easy operation are the main advantages of the synthesized adsorbent. Moreover, the detailed study of adsorption behavior on real samples confirmed that synthesized MNPs are beneficial in industrial applications for the removal of Carmoisine from wastewater.

Acknowledgments

The authors are grateful to the Research Council of the University of Guilan and Rasht Branch of Islamic Azad University for the partial support of this study.

References

[1] T.W. Seow, C.K. Lim, Removal of dye by adsorption: a review, Int. J. Appl. Eng. Res., 11 (2016) 2675–2679.

[2] W.J. Zhang, K.J. Huang, A review of recent progress in molybdenum disulfide-based supercapacitors and batteries, Inorg. Chem. Front., 4 (2017) 1602–1620.

[3] Y.H. Wang, K.J. Huang, X. Wu, Recent advances in transition-metal dichalcogenides based electrochemical biosensors: a review, Biosens. Bioelectron., 97 (2017) 305–316.

[4] Q. Liu, J. Shen, X. Yang, T. Zhang, H. Tang, 3D reduced graphene oxide aerogel-mediated Z-scheme photocatalytic system for highly efficient solar-driven water oxidation and removal of antibiotics, Appl. Catal., B, 232 (2018) 562–573.

[5] H.L. Shuai, X. Wu, K.J. Huang, Z.B. Zhai, Ultrasensitive electrochemical biosensing platform based on spherical silicon dioxide/molybdenum selenide nanohybrids and triggered hybridization chain reaction, Biosens. Bioelectron., 94 (2017) 616–625.

[6] Y. Fu, Z. Li, Q. Liu, X. Yang, H. Tang, Construction of carbon nitride and MoS_2 quantum dot 2D/0D hybrid photocatalyst: direct Z-scheme mechanism for improved photocatalytic activity, Chin. J. Catal., 38 (2017) 2160–2170.

[7] K. Wang, J. Fu, S. Wang, M. Gao, J. Zhu, Z. Wang, Q. Xu, Polydopamine-coated magnetic nanochains as efficient dye adsorbent with good recyclability and magnetic separability, J. Colloid Interface Sci., 516 (2018) 263–273.

[8] Z. Khan, O. Bashir, M.N. Khan, T.A. Khan, S.A. Al-Thabaiti, Cationic surfactant assisted morphology of Ag@Cu, and their catalytic reductive degradation of Rhodamine B, J. Mol. Liq., 248 (2017) 1096–1108.

[9] G. Tang, W. Chen, X. Wan, F. Zhang, J. Xu, Construction of magnetic Fe_3O_4 nanoparticles coupled with flower-like $MoSe_2$ nanosheets for efficient adsorptive removal of methylene blue, Colloids Surf., A, 587 (2020) 124291, doi: 10.1016/j.colsurfa.2019.124291.

[10] Z. Kiayi, T.B. Lotfabad, A. Heidarinasab, F. Shahcheraghi, Microbial degradation of azo dye carmoisine in aqueous medium using *Saccharomyces cerevisiae* ATCC 9763, J. Hazard. Mater., 373 (2019) 608–619.

[11] E. Sharifpour, M. Ghaedi, A. Asfaram, M. Farsadrooh, E.A. Dil, H. Javadian, Modeling and optimization of ultrasound-assisted high performance adsorption of Basic Fuchsin by starch-capped zinc selenide nanoparticles/AC as a novel composite using response surface methodology, Int. J. Biol. Macromol., 152 (2020) 913–921.

[12] C.H. Liu, J.S. Wu, H.C. Chiu, S.Y. Suen, K.H. Chu, Removal of anionic reactive dyes from water using anion exchange membranes as adsorbers, Water Res., 41 (2007) 1491–1500.

[13] B. Prasad, C. Ghosh, A. Chakraborty, N. Bandyopadhyay, R. Ray, Adsorption of arsenite (As^{3+}) on nano-sized Fe_2O_3 waste powder from the steel industry, Desalination, 274 (2011) 105–112.

[14] K. Dutta, S. Mukhopadhyay, S. Bhattacharjee, B. Chaudhuri, Chemical oxidation of methylene blue using a Fenton-like reaction, J. Hazard. Mater., 84 (2001) 57–71.

[15] Y. Wang, Z. Wang, S. Wang, Z. Chen, J. Chen, Y. Chen, J. Fu, Magnetic poly(cyclotriphosphazene-co-4,4′-sulfonyldiphenol) nanotubes modified with glacial acetic acid for removing methylene blue: adsorption performance and mechanism, Eur. Polym. J., 120 (2019) 1–10, doi: 10.1016/j.eurpolymj.2019.08.025.

[16] M.N. Khan, O. Bashir, T.A. Khan, S.A. Al-Thabaiti, Z. Khan, CTAB capped synthesis of bio-conjugated silver nanoparticles and their enhanced catalytic activities, J. Mol. Liq., 258 (2018) 133–141.

[17] H. Mittal, A. Maity, S.S. Ray, Synthesis of co-polymer-grafted gum karaya and silica hybrid organic–inorganic hydrogel nanocomposite for the highly effective removal of methylene blue, Chem. Eng. J., 279 (2015) 166–179.

[18] J. Fu, Q. Xin, X. Wu, Z. Chen, Y. Yan, S. Liu, M. Wang, Q. Xu, Selective adsorption and separation of organic dyes from aqueous solution on polydopamine microspheres, J. Colloid Interface Sci., 461 (2016) 292–304.

[19] J. Fu, Z. Chen, M. Wang, S. Liu, J. Zhang, J. Zhang, R. Han, Q. Xu, Adsorption of methylene blue by a high-efficiency adsorbent (polydopamine microspheres): kinetics, isotherm, thermodynamics and mechanism analysis, Chem. Eng. J., 259 (2015) 53–61.

[20] J. Fu, J. Zhu, Z. Wang, Y. Wang, S. Wang, R. Yan, Q. Xu, Highly-efficient and selective adsorption of anionic dyes onto hollow polymer microcapsules having a high surface-density of amino groups: isotherms, kinetics, thermodynamics and mechanism, J. Colloid Interface Sci., 542 (2019) 123–135.

[21] D. Mehta, S. Mazumdar, S.K. Singh, Magnetic adsorbents for the treatment of water/wastewater—a review, J. Water Process Eng., 7 (2015) 244–265.

[22] Y. Wang, C. Lin, Z. Wang, Z. Chen, J. Chen, Y. Chen, S. Liu, J. Fu, Magnetic hollow poly(cyclotriphosphazene-co-4,4′-sulfonyldiphenol)-Fe_3O_4 hybrid nanocapsules for adsorbing Safranine T and catalytic oxidation of 3,3′,5,5′-tetramethylbenzidine, J. Colloid Interface Sci., 556 (2019) 278–291.

[23] W. Zhao, B. Cui, H. Peng, H. Qiu, Y. Wang, Novel method to investigate the interaction force between etoposide and APTES-functionalized Fe_3O_4@nSiO_2@mSiO_2 nanocarrier for drug loading and release processes, J. Phys. Chem. C, 119 (2015) 4379–4386.

[24] D.W. Wang, X.M. Zhu, S.F. Lee, H.M. Chan, H.W. Li, S.K. Kong, C.Y. Jimmy, C.H. Cheng, Y.X.J. Wang, K.C.F. Leung, Folate-conjugated Fe_3O_4@SiO_2@gold nanorods@ mesoporous SiO_2 hybrid nanomaterial: a theranostic agent for magnetic resonance imaging and photothermal therapy, J. Mater. Chem. B, 1 (2013) 2934–2942.

[25] M. Yang, L. Gao, K. Liu, C. Luo, Y. Wang, L. Yu, H. Peng, W. Zhang, Characterization of $Fe_3O_4/SiO_2/Gd_2O(CO_3)_2$ core/shell/shell nanoparticles as T1 and T2 dual mode MRI contrast agent, Talanta, 131 (2015) 661–665.

[26] D. Yimin, Z. Jiaqi, L. Danyang, N. Lanli, Z. Liling, Z. Yi, Z. Xiaohong, Preparation of Congo red functionalized Fe_3O_4@SiO_2 nanoparticle and its application for the removal of methylene blue, Colloids Surf., A, 550 (2018) 90–98.

[27] S. Toutounchi, S. Shariati, K. Mahanpoor, Application of magnetic ordered mesoporous carbon nanocomposite for the removal of ponceau 4R using factorial experimental design, Silicon, 13 (2021) 1561–1573.

[28] K. Cui, B. Yan, Y. Xie, H. Qian, X. Wang, Q. Huang, Y. He, S. Jin, H. Zeng, Regenerable urchin-like Fe_3O_4@PDA-Ag hollow microspheres as catalyst and adsorbent for enhanced removal of organic dyes, J. Hazard. Mater., 350 (2018) 66–75.

[29] S. Shariati, M. Khabazipour, F. Safa, Synthesis and application of amine functionalized silica mesoporous magnetite nanoparticles for removal of chromium(VI) from aqueous solutions, J. Porous Mater., 24 (2017) 129–139.

[30] S.M.S. Danesh, H. Faghihian, S. Shariati, Sulfonic acid functionalized magnetite nanoporous-KIT-6 for removal of methyl green from aqueous solutions, J. Nano Res., 52 (2018) 54–70.

[31] K. Nadafi, M. Vosoughi, A. Asadi, M.O. Borna, M. Shirmardi, Reactive Red 120 dye removal from aqueous solution by adsorption on nano-alumina, J. Water Chem. Technol., 36 (2014) 125–133.

[32] M. Tempkin, V. Pyzhev, Kinetics of ammonia synthesis on promoted iron catalyst, Acta Phys. Chim. USSR, 12 (1940) 327.

[33] F. Ghorbani, S. Kamari, Core-shell magnetic nanocomposite of Fe_3O_4@SiO_2@NH_2 as an efficient and highly recyclable adsorbent of methyl red dye from aqueous environments, Environ. Technol. Innovation, 14 (2019) 1–16, doi: 10.1016/j.eti.2019.100333.

[34] M.M. Galangash, Z.N. Kolkasaraei, A. Ghavidast, M. Shirzad-Siboni, Facile synthesis of methyl propylaminopropanoate functionalized magnetic nanoparticles for removal of acid red 114 from aqueous solution, RSC Adv., 6 (2016) 113492–113502.

[35] P. Wang, X. Wang, S. Yu, Y. Zou, J. Wang, Z. Chen, N.S. Alharbi, A. Alsaedi, T. Hayat, Y. Chen, Silica coated Fe_3O_4 magnetic nanospheres for high removal of organic pollutants from wastewater, Chem. Eng. J., 306 (2016) 280–288.